Journal of Hazardous Materials 378 (2019) 120721

Contents lists available at ScienceDirect

Journal of Hazardous Materials

journal homepage: www.elsevier.com/locate/jhazmat

Development of a magnetic core-shell Fe_3O_4@TA@UiO-66 microsphere for removal of arsenic(III) and antimony(III) from aqueous solution

Pengfei Qi[a,*], Rong Luo[b], Thomas Pichler[c], Jianqiang Zeng[a], Yan Wang[d], Yuhua Fan[b,*], Kunyan Sui[a,*]

[a] State Key Laboratory of Bio-Fiber and Eco-Textiles, College of Materials Science and Engineering, Collaborative Innovation Center for Marine Biobased Fibers and Ecological textiles, Institute of Marine Biobased Materials, Qingdao University, Qingdao 266071, China
[b] Key Laboratory of Marine Chemistry Theory and Technology, Ministry of Education, College of Chemistry and Chemical Engineering, Ocean University of China, Qingdao 266100, China
[c] Geochemistry & Hydrogeology, Department of Geosciences, University of Bremen, Klagenfurter Straße, 28359 Bremen, Germany
[d] Department of Chemical Engineering College of Applied Technology, Qingdao University, Qingdao 266061, China

GRAPHICAL ABSTRACT

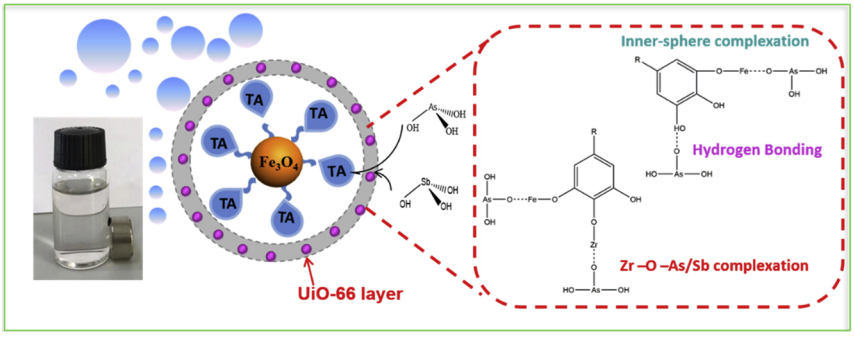

ARTICLE INFO

Keywords:
Remediation
Magnetic microsphere
As(III) and Sb(III)
Complexation and hydrogen bonding

ABSTRACT

Removal of trivalent species of As and Sb from wastewater is crucial due to their more toxic and mobile properties. In this study, a novel magnetic core-shell microsphere Fe_3O_4@TA@UiO-66 was developed via in-situ crystal growth of UiO-66 around the magnetic Fe_3O_4 modified by Tannic Acid (TA). Characterization of the microsphere by transmission electron microscopy (TEM) and X-ray diffraction spectroscopy (XRD) confirmed that UiO-66 was adhered on the surface of Fe_3O_4 functionalized by TA. Adsorption experiments showed that the magnetic Fe_3O_4@TA@UiO-66 had high adsorption capacity for As(III) and Sb(III) and could be rapidly separated from aqueous media within two minutes after treatment. The adsorption kinetics and adsorption isotherms were described well by the pesudo-second order model and Langmuir model, respectively. In addition, the composite exhibited excellent removal performance for As(III) and Sb(III) in a broad solution chemistry environment, including pH and co-existing anions. Based on X-ray photoelectron spectroscopy (XPS) and Fourier transform infrared spectroscopy (FTIR) measurement, we proposed that the removal mechanism was mainly controlled through a synergistic interaction of surface complexation and hydrogen bonding. This study indicates the potential of the magnetic microsphere to be used as an effective material for the removal of As(III) and Sb(III) from water.

* Corresponding authors.
E-mail addresses: pengfei@uni-bremen.de (P. Qi), fanyh@ouc.edu.cn (Y. Fan), sky@qdu.edu.cn (K. Sui).

https://doi.org/10.1016/j.jhazmat.2019.05.114
Received 8 March 2019; Received in revised form 30 May 2019; Accepted 31 May 2019
Available online 01 June 2019
0304-3894/

1. Introduction

Arsenic (As) and antimony (Sb) contamination in aqueous media has attracted worldwide attention, whether as a result of geogenic processes or their increasing industrial consumption during production of ceramics, flame retardants and alloys [1,2]. Both As and Sb are classified as toxic metalloids and are detrimental for human health and well-being [3,4]. The maximum contamination levels (MCLs) specified by the world health organization (WHO) for As and Sb in drinking water are 10.0 μg/L and 5.0 μg/L, respectively [5]. In aqueous solution, As(III) is stable as a neutral form of $As(OH)_3$ in the pH range of 0 to 9, and the dominant Sb(III) species is uncharged pyramidal antimonous acid $Sb(OH)_3$ in a wide pH range from 2 to 11 under anoxic conditions [6]. While As(V) and Sb(V) species are mostly present as oxyanions under oxic conditions. Generally, the trivalent species are considered more toxic and soluble than the pentavalent species. Hence, the removal of As(III) and Sb(III) from aqueous solutions should be a priority due to their greater mobility and toxicity.

Various types of adsorbents have been employed as means of heavy metal ions removal from aqueous media, including natural organic compounds [7], metal oxides [8–11], clays [12], potassium ferrate [13], nano titania composites [14–16], and metal-organic frameworks (MOFs) [17–21]. Among these materials, MOFs have attracted particular attention and have vast potential applications in adsorption, separation, sensors and catalysis due to their large surface area, abundant porosity, and easy tenability of structures [22–24]. For example, Audu et al. succeed to tailor the structure of a UiO derivative for the coordination of As(V) at the node and bind neutral As(III) with the linkers at the same time [23]. UiO-66 based MOFs is a kind of Zr-MOF and are gaining attention in water treatment due to its hydrophilicity and small aperture sizes [25]. UiO-67, for example, has successfully removed p-Arsanilic Acid [26], selenium [27], and arsenic [28] from water, mainly depending on π–π stacking interaction, electrostatic interaction, and surface coordination. Thus the adsorption by UiO derivatives could be a most promising methodology for the removal of toxic elements such as As and Sb. Nonetheless, the MOF particles are usually applied in the form of powers, which often require complicated separation procedures from aqueous media and cause material loss during separation, which partly impeded the development of MOFs for water treatment.

The problems arising from difficult separation could be overcome by using magnetic nanoparticles. They still have large surface area and are easily separated using a magnetic procedure [29]. Thus, the configuration of a magnetic-core and MOFs-shell synergistically combines the advantages of magnetic particles and MOFs, which could be a promising material for the remediation of heavy metals. For example, a magnetic nanocomposite Fe_3O_4@ZIF-8 was designed for efficient adsorption of UO_2^{2+} [30]. However, a MOF-containing magnetic composite material is still rare for the simultaneous capture of As and Sb.

As part of this study, a magnetic core-shell nanocomposite was designed and prepared, where Fe_3O_4 and UiO-66 were connected by polyphenol tannic acid (TA) as a modifier and bridge. TA, a low-cost and environmental friendly polyphenol, has already gained great interest as a hydrophilic surface modification due to its nontoxic, colourless, easily accessible and biodegradable properties [31]. Thus the self-prepared Fe_3O_4 was firstly modified and functionalized by TA [32]. Then a nanocomposite was prepared via in-situ crystal growth of UiO-66 around the surface of Fe_3O_4@TA, where abundant hydroxyl groups coordinated with zirconium ions and further reacted with organic ligands [33]. The addition of TA may prevent the aggregation the magnetic core, improve the dispersion stability, and provide additional adsorption sites benefiting the removal of As(III) and Sb(III) [34]. More importantly, the composite was easily separated from solutions in a magnetic field. Following successful generation of the microsphere, the As(III) and Sb(III) adsorption capacity and mechanisms were evaluated and studied.

2. Experimental section

2.1. Materials

All chemicals used in this study were of analytical grade. Tannic acid (TA) and Zirconium chloride ($ZrCl_4$) were purchased from Shanghai Aladdin Chemistry Co. Ferrous chloride tetrahydrate ($FeCl_2{\cdot}4H_2O$), sodium hydroxide (NaOH), ammonia ($NH_3{\cdot}H_2O$) and P-Phthalic acid ($C_8H_6O_4$) were purchased from Sinopharm Co. Ltd. Stock 1000 mg/L Sb(III) solution was prepared by dissolving potassium antimonyl tartrate trihydrate ($C_8H_4K_2O_{12}Sb_2{\cdot}3H_2O$, Sigma-Aldrich) in deionized water. Another stock solution of As(III) was prepared by dissolving $NaAsO_2$ (Sigma-Aldrich) in deionized water. The working solutions were freshly prepared each time by diluting the stock solutions to required concentrations.

2.2. Synthesis of Fe_3O_4@TA@UiO-66 nanosphere

The Fe_3O_4 nanoparticles were firstly synthesized by a co-precipitation method. A 0.3 M solution of $FeCl_2{\cdot}4H_2O$ was heated the to 90 °C under N_2 protection, then NaOH solution (17 wt%) was added dropwise under constant stirring until a milky suspension of $Fe(OH)_2$ was began to form. Then the nitrogen gas was replaced by regular air and as a result of atmospheric oxygen the suspension began to oxidize. During that process, the milky $Fe(OH)_2$ suspension turned first to dark green and finally to black. In the subsequent step, the black precipitates were separated from the solution using a permanent magnet and washed repeatedly with deionized water and ethanol. Finally, the obtained powder was dried at 80℃ in vacuum for further use.

Secondly, Fe_3O_4@TA was obtained by reacting 100 mg of ammoniated self-prepared Fe_3O_4 with 100 mg TA in 30 mL deionized water under constant stirring at room temperature for 24 h. The products were collected using a permanent magnet then washed and dried. At last, the freshly precipitated Fe_3O_4@TA (0.1 g), $ZrCl_4$ (1 mmol, 0.233 g) and terephthalic acid (1 mmol, 0.166 g) were dissolved in 50 mL DMF under ultrasonic vibration for 30 min and then mechanically stirred at room temperature for 4 h. Then the final mixture was transferred to a Teflon-lined stainless steel vessel, heated to 140 °C for 18 h. After cooling to room temperature, the precipitated were recovered using a permanent magnet, washed with DMF and ethanol and then dried for further characterization and evaluation.

2.3. Batch experiments

The adsorption performance of Fe_3O_4@TA@UiO-66 were performed in sealed polyethylene tubes at room temperature in a batch mode. Specifically, adsorption isotherm studies were conducted at initial concentrations ranging from 1 to 40 mg/L, with a constant adsorbent dosage of 0.2 g/L. To obtain information on adsorption kinetics, a dosage of 0.2 g/L of adsorbent was added to a 50 mL solution containing 10 mg/L As(III) and Sb(III) solutions, respectively. The suspensions were shaken for 5 min to 24 h. The effect of solution chemistry on the removal performance of As(III) and Sb(III) were also studied, including pH, co-existing anions and ionic strength. Specifically, the effect of pH was investigated in a broad pH range from 3 to11, and the pH values were adjusted by adding either HCl or NaOH solutions. Co-existing anions, including CO_3^{2-}, SO_4^{2-}, SiO_3^{2-} and PO_4^{3-} with concentrations of 10 mg/L, were mixed with 10 mg/L As(III) and Sb(III) solution, respectively. The mixtures were horizontally shaken in a shaking water bath at room temperature. After equilibrium, the solids were magnetically separated from the aqueous solutions. The concentrations of supernatants were determined by inductively coupled plasma optical emission spectrometer (ICP-OES, Avio 200). All the experiment were performed in triplicates and the average results were reported.

2.4. Characterization

The morphologies of the composite particles were studied using a transmission electron microscopy (TEM, JEM-1200EX electron microscope, JEOL, Japan). The structures and interactions of the samples before and after adsorption were monitored using a Fourier transform infrared spectrometer (FTIR) and X-ray photoelectron spectroscopy (XPS). X-ray powder diffraction (PXRD) patterns were collected with a PANalytical X'Pert Pro diffractometer using Cu-Kα radiation and scanning from 5° to 80° 2 θ to determine the crystal structure of samples. The zeta potential of the precipitates in distilled water was determined by a zetasizer instrument at ambient temperature. The pore size distribution and surface area were determined with the Brunauer-Emmett-Teller (BET) N_2 adsorption/desorption method.

3. Results and discussion

3.1. Synthesis and characterization

The schematic of the in situ crystal growth of UiO-66 MOF particles around magnetic Fe_3O_4@TA is presented in Fig. 1 as well as the TEM images of the corresponding products. As shown in Fig. 1a, the magnetic Fe_3O_4 was modified by TA, where the TA support was beneficial for impeding the spontaneous aggregation and enhancing the dispersibility of Fe_3O_4 through self-assembly of the active phenol hydroxyl groups. The UiO-66 MOF nanoparticles were in situ formed around the magnetic Fe_3O_4@TA. The size of the Fe_3O_4@TA@UiO-66 nanocomposite was approximately in the range of 200 ± 10 nm. The TEM image shows that the morphology of the microsphere was spheric and possessed a distinct core-shell structure, where a UiO-66 shell wrapped around the intermediate product of Fe_3O_4@TA with a thickness about 13 nm (Fig. 2b). The shell of the spheric composite consists of a cubic framework of $Zr_6O_4(OH)_4$ cluster (Fig. S1).

The structure of the products was determined by the XRD analysis. The XRD patterns of the Fe_3O_4@TA@UiO-66 particles exhibited typical characteristic peaks, which corresponded well to the simulated UiO-66 crystal structure (Fig. 2a). After modifying the Fe_3O_4 core with hydroxyl groups and coating with TA, the diffraction peaks of UiO-66 could still be identified, suggesting that the framework structure of UiO-66 was preserved. In addition, the microstructure of the synthesized microsphere was analyzed by FT-IR spectrum (Fig. 2b). The bands at 1390 and 1580 cm^{-1} were ascribed to the asymmetric and symmetric stretching vibrations of O—C—O in terephthalic linkers [35]. And the band at approximately 540 cm^{-1} is related to the Zr—O bond, which was further confirmed by the XPS analysis (Fig. 5a). These results indicate the successfully crystal growth of UiO-66 on the surface of Fe_3O_4@TA.

The specific surface area of Fe_3O_4@TA@UiO-66 microsphere determined by N_2 adsorption-desorption isotherms was 130.3 m^2/g (Fig. 2c). And the UiO-66 shell layer has a structure with abundant of nanopores, where the inset shows the pore size distribution determined by the BJH analysis based on the desorption data. It showed that the average pore diameter was about 4 nm, and total pore volume was 0.18 cm^3/g. Compared to pristine UiO-66, such a decrease in surface area and pore volume of Fe_3O_4@TA@UiO-66 could be ascribed to the encapsulation of Fe_3O_4 nanoparticles into UiO-66 MOF nanoparticles [22]. Thus, the as-prepared Fe_3O_4@TA@UiO-66 with its magnetic property as well as its large surface area and porous structure may prove to be an ideal adsorbent for remediation of As(III) and Sb(III) and potentially other metals.

3.2. Sorption kinetics of As(III) and Sb(III)

Kinetics adsorption experiment were carried out to investigate adsorption rate at the initial concentration of 10 mg/L as shown in Fig. 2a and b, and almost more than 80% of As(III) and Sb(III) was adsorbed in less than 2 h and reached equilibrium within 24 h. And a slight slower Sb(III) adsorption could be ascribed to partial oxidation of Sb(III) in the presence of dissolved oxygen. All the experimental kinetics data followed the pseudo-second-order model well, and the kinetics parameters were calculated and shown in Table S2. It indicates that the chemical sorption controlled the sorption rate of As(III) and Sb(III), and the available active sites determined the adsorption capacity [36]. Remarkably, after the adsorption reach equilibrium, the adsorbent can be completely separated from aqueous solutions in two minutes, as shown in the inset of Fig. 3a and b. It suggest that the magnetic core-shell microsphere has a potential application on the removal of As(III) and Sb (III) from water based on UiO-66 MOFs.

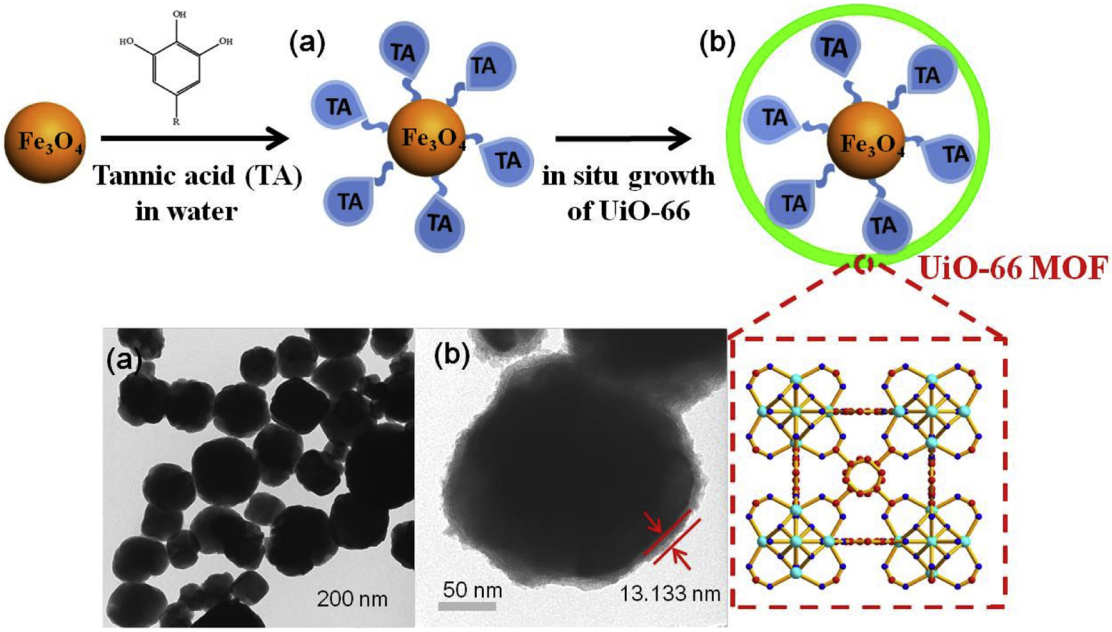

Fig. 1. Schematic showing the synthesis of magnetic microsphere. (a) TEM images of the surface modified of Fe_3O_4 by tannic acid (TA). (b) UiO-66 MOF particles in situ formed around the magnetic Fe_3O_4@TA.

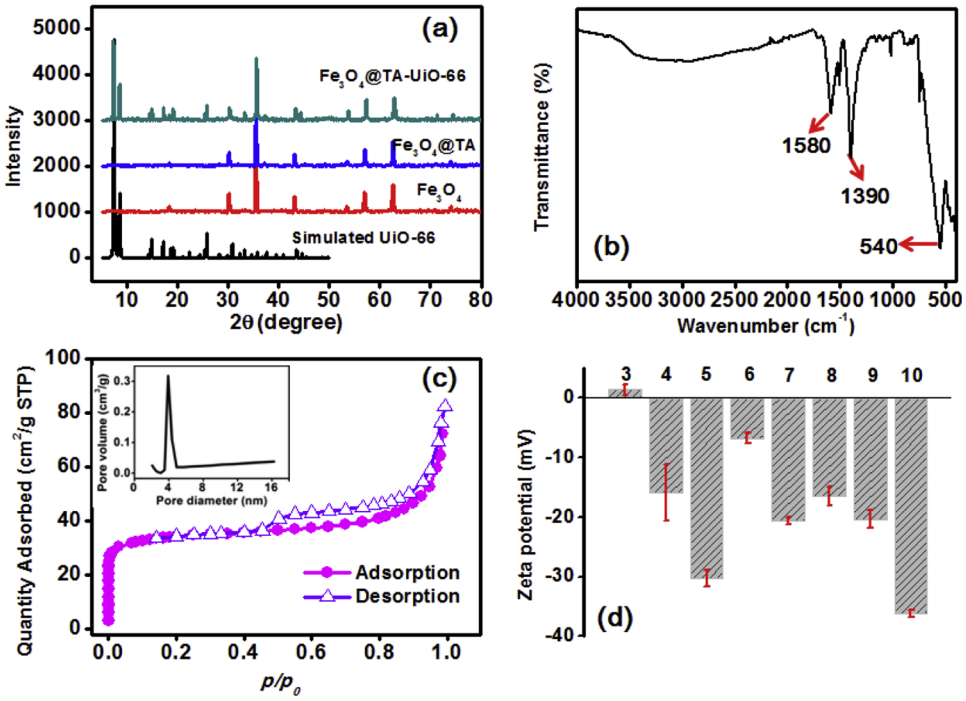

Fig. 2. (a) PXRD patterns of simulated UiO-66, Fe_3O_4, Fe_3O_4@TA, and Fe_3O_4@TA@UiO-66; (b) FTIR spectrum of synthesized Fe_3O_4@TA@UiO-66; (c) N_2 adsorption-desorption measurement of Fe_3O_4@TA@UiO-66; (d) Zeta potentials of Fe_3O_4@TA@UiO-66 as a function of pH values.

3.3. Batch equilibrium adsorption isotherm

Adsorption isotherms of Fe_3O_4@TA@UiO-66 toward As(III) and Sb (III) are shown in Fig. 3c. The Langmuir and Freundlich models were used to fit the adsorption isotherm data. Langmuir model was preferred for adsorption of As(III) and Sb(III) with the correlation coefficient $R^2 > 0.99$ (Table S2), suggesting that the adsorption procedure for both As(III) and Sb(III) is monolayer. The maximum adsorption capacity of As(III) was higher than Sb(III) calculated from Langmuir model. This observation could be explained that As(III) with a smaller atomic radius is preferred to be located in the aperture of the nanopores of UiO-66 than Sb(III), where both of them are tetrahedral linked with three hydroxyl radicals. In addition, the active hydroxyl group attached to Fe_3O_4 could facilitate the formation of inner-sphere complexation between Fe and As(III) [37]. Although some of pure UiO-66 MOFs exhibited higher capacity for Sb(III) than the as-prepared composite of Fe_3O_4@TA@UiO-66 [38], overall, it still showed comparable uptake performance towards for both As(III) and Sb(III) species. Especially it exhibited excellent removal capacity for As(III) (97.8 mg/g), and its unique magnetism endow it to have an outstanding real application.

3.4. Effect of solution chemistry

The effect of pH on the removal of As(III) and Sb(III) was studied in order to access the role of electrostatic attraction. As shown in Fig. 3d, the adsorption behavior of As(III) and Sb(III) displayed a similar trend and their adsorption behavior was more or less pH independent. The possible reason may be related to the species distribution of As(III) and Sb(III), where both of the them are stable as a neural form of H_3AsO_3 and H_3SbO_3 in a wide pH range from 2 to 9 under anoxic conditions [39]. Zeta potential measurements were performed to access the function of electrostatic attraction (Fig. 2d), where the point of zero charge (pH_{pzc}) for Fe_3O_4@TA@UiO-66 was at approximately 3. Especially for Sb(III), the maximum adsorption capacity almost occurred at the pH_{pzc}. And for As(III), the adsorption capacity occurred at the pH_{pzc} was similar to that adsorbed if the surface charge of the adsorbate is negatively charged, suggesting that the adsorption of the two species is not related and controlled by electrostatic attraction.

The removal performance of As(III) and Sb(III) in the presence of common anions such as CO_3^{2-}, SO_4^{2-}, SiO_3^{2-} and PO_4^{3-} were also studied, respectively. As shown in Fig. 3e, none of the four oxyanions had a distinct influence on the uptake of As(III) and Sb(III) by Fe_3O_4@TA@UiO-66 at experimental conditions, which are similar to previous studies [40]. The results suggest that the driving force for the both species is chemical sorption. In addition, the removal of As(III) and Sb(III) were hardly be affected by the ionic strength with an increasing concentration of NaCl (Fig. 3f), suggesting that the two species are bound on the surface sites via the formation of inner-sphere complexes [41]. Overall, the magnetic composite of Fe_3O_4@TA@UiO-66 exhibited pH independence and good anti-interference ability, and it could be as a promising adsorbent to treat wastewaters.

3.5. Removal mechanism

To get insight into the synergistic effect of the three components on the adsorption mechanism, the surface chemical environment of Fe_3O_4@TA@UiO-66 before and adsorption were studied by XPS and FTIR measurements, respectively. As shown in Fig. 4a, the peaks corresponding to Zr 3s, Zr 3p, and Zr 3d are observed, indicating the successful situ crystal growth of UiO-66 around the modified magnetic Fe_3O_4. And the appearance of As3d and Sb3d confirmed the adsorption of As and Sb species.

The detail information of Zr 3d peak is shown in Fig. 4b. The peaks located at approximately 182.8 and 185 eV correspond to Zr−O bonds [38], which were shifted after the adsorption of As(III) and Sb(III). And the other two peaks at the binding energy of 183.4 and 185.7 eV correspond to the metallic Zr−Zr bonds, which were also shifted somewhat in order to keep the framework of the unit cell of UiO-66 MOFs. However, the intensity of Zr−Zr peak was almost unchanged before and after adsorption. Thus it suggests that only Zr−O bonds play an important role for the adsorption of As(III) and Sb(III). The FTIR data further confirmed that the adsorption of As(III) and Sb(III) facilitated by

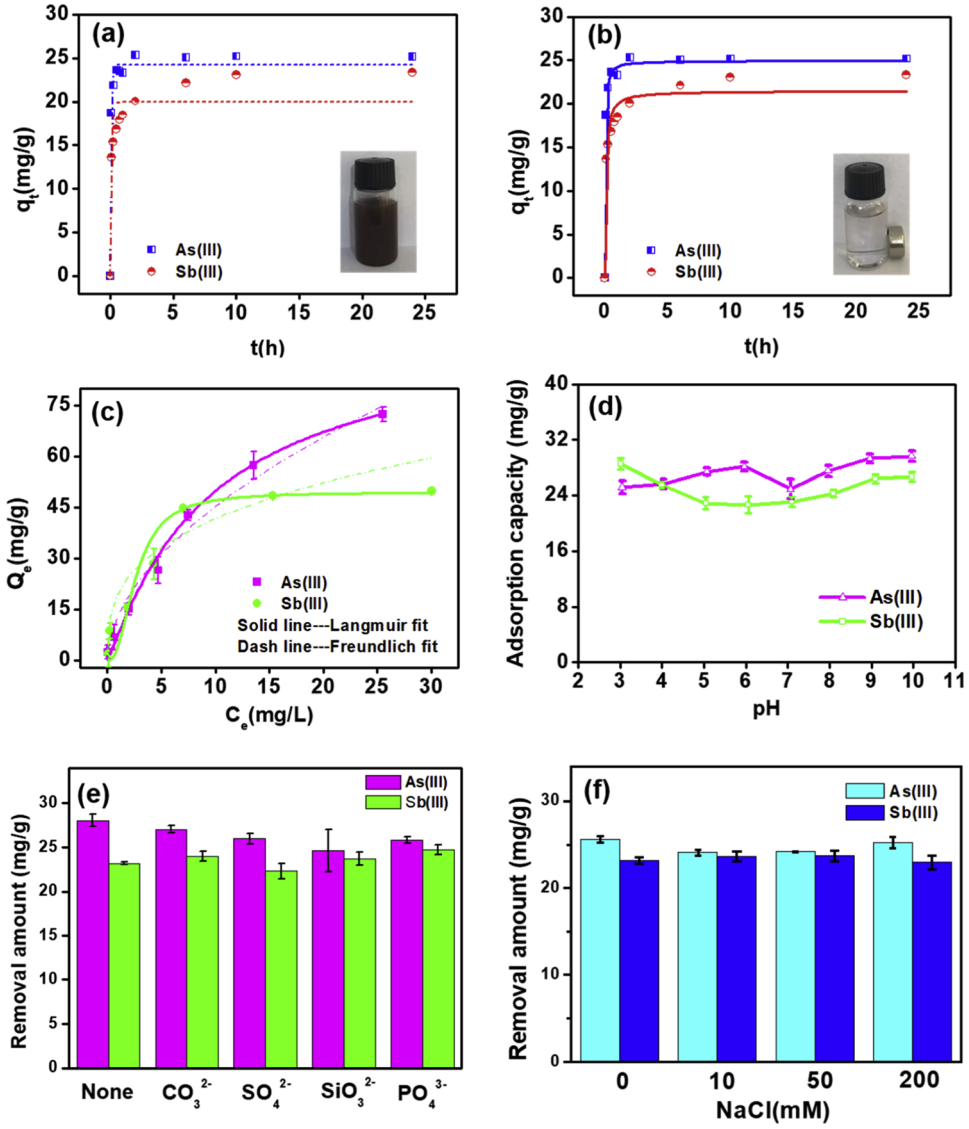

Fig. 3. Adsorption performance of As(III) and Sb(III) in singular system on Fe_3O_4@TA@UiO-66. Adsorption kinetic data and pseudo-first order fit (a) and pseudo-second order fit (b), where the dosage of adsorbent was 0.2 g/L and solution pH was 7. (c) Equilibrium data with the initial concentration range from 0.5 to 40 mg L^{-1} at room temperature, and Langmuir and Freundlich fit for the adsorption data; Effect of pH values (d) and common anions (e) and ionic strength (f) on the removal performance of As(III) and Sb(III).

the complexation of Zr—O—As or Zr—O—Sb. This is documented in the FTIR spectrum (Fig. 5), through the appearance of the characteristic peaks around 745 and 550 cm^{-1}, which correspond to the stretching vibration of OH and CH, and Zr—O, respectively [42]. After As(III) and Sb(III) adsorption, the band at 550 cm^{-1} shifted marginally and became less intense.

Notably, after Sb(III) removal, two typical peaks of Sb $3d_{3/2}$ and $Sb3d_{5/2}$ located at approximately 540.1 and 531.8 eV in the Sb 3d spectrum were observed (Fig. 4c). The appearance of $Sb3d_{5/2}$ confirmed that Sb(III) was indeed adsorbed on the surface of Fe_3O_4@TA@UiO-66. At the same time, the presence of another peak corresponding to $Sb3d_{3/2}$ indicated the existence of Sb(V), suggesting that partial of adsorbed Sb (III) was converted to Sb(V), and the formed Sb(V) was still bound on the surface sites. It was reported that Sb(III) was oxidized more easily at a lower Eh than As(III) [43]. And we examined the kinetics of the speciation change during the adsorption process of Sb(III) on the iron-based materials in our previous studies [44]. Only trace amount of Sb (V) (less than 0.05 mg/L) was observed in solutions under non-acidic conditions. Moreover, the oxidation of Sb(III) could be retarded by tannic acid as a weak reductant. Thus the adsorption of the formed Sb (V) could be negligible comparing to the studied concentration range of Sb(III).

The deconvolution of O1s peak showed four types of oxygen bonds, and the peak at approximately 532 eV was assigned to —OH group [45], which was shifted significantly to high binding energy especially after As(III) adsorption, indicating a stronger electron attracting property of —OH group. It suggests that hydrogen bonding interaction could be involved between the phenol hydroxyl groups and the adsorbed species, which plays a synergistic effect on the adsorption of adsorbed species. Furthermore, the change of the Fe—O bond confirmed the involvement of inner-sphere complexation for the adsorption of As(III) and Sb(III). It was also identified that the inner-sphere complexation was formed between a magnetic surface and As species [36]. And the hydroxyl group on the surface of iron may be beneficial for the formation of inner-sphere complexation. The above results suggest that the addition of TA not only facilitate the connection of UiO-66 MOFs with the magnetic Fe_3O_4 core, but also enhanced the adsorption capacity of the adsorbed species due to hydrogen bonding and inner-sphere complexation.

Based on the aforementioned analyses, results and discussion, the

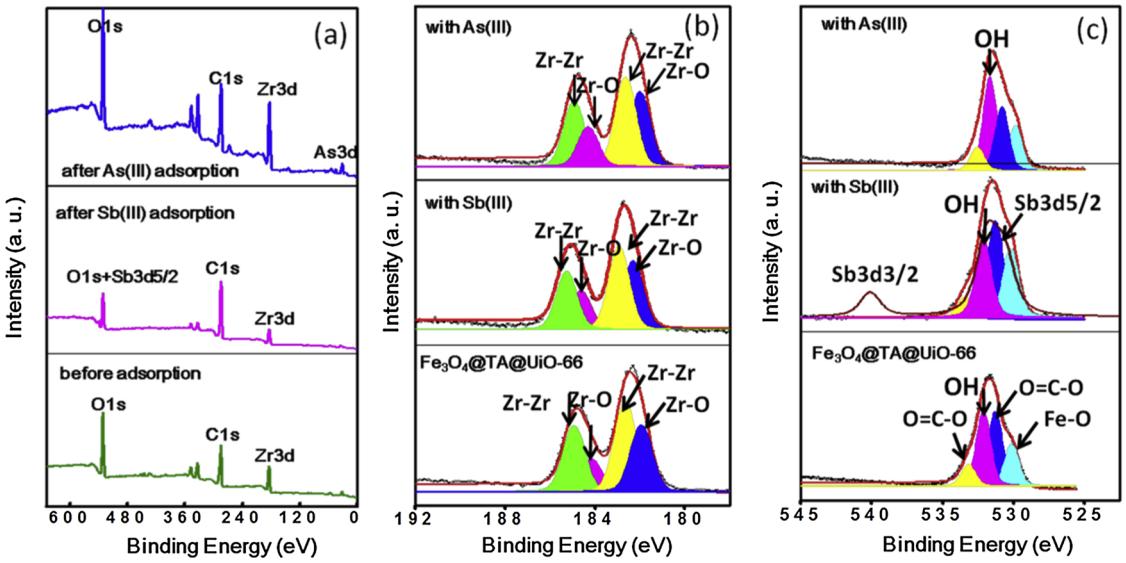

Fig. 4. XPS characterization of Fe_3O_4@TA@UiO-66 before and after As(III) and Sb(III) adsorption. (a) XPS survey spectrum. (b). Zr 3d and (c) O 1s +Sb 3d.

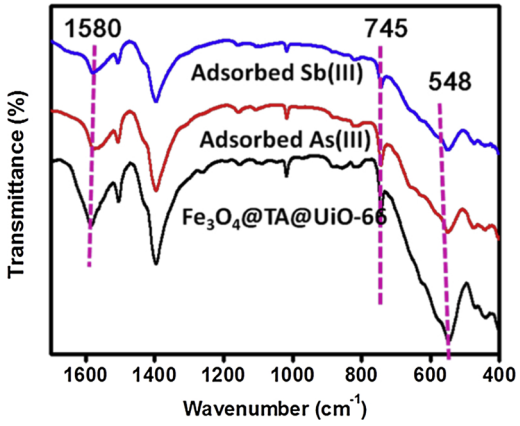

Fig. 5. FTIR spectrum of Fe_3O_4@TA@UiO-66 (black) and As(III) containing Fe_3O_4@TA@UiO-66 (red) and Sb(III) containing Fe_3O_4@TA@UiO-66 (blue). (For interpretation of the references to colour in this figure legend, the reader is referred to the web version of this article.)

likely removal mechanism of As(III) and Sb(III) by Fe_3O_4@TA@UiO-66 is illustrated in Fig. 6, which could be controlled by the synergistic effect of surface complexation and hydrogen bonding. Noteworthy, here the removal mechanism for As(III) and Sb(III) was mainly discussed depending on their dominant existing forms of $As(OH)_3$ and $Sb(OH)_3$ in a wide pH range. Specifically, the non-charged species of As (III) and Sb(III) were adsorbed onto the surface sites via surface complexation involving Zr—O and Fe—O bonds. And the abundant hydroxyl groups originating from TA could facilitate the uptake of As(III) and Sb(III) through the formation of hydrogen bonds. Notably, partial of the adsorbed Sb(III) was converted to Sb(V), which were still attached on the surface sites. Following adsorption the adsorbent can be separated from the aqueous solution rapidly within two minutes using a magnet. This suggest that the modified Fe_3O_4 by polyphenol not only promotes the application of UiO-66 in water treatment but also synergistically enhance the removal capacity.

4. Conclusion

In this work, a magnetic core-shell microsphere, was synthesized for the first time via in-stiu crystal growth of UiO-66 around a core of Fe_3O_4@TA. And the removal of As(III) and Sb(III) from solutions by Fe_3O_4@TA@UiO-66 was studied in detail. The surface modification by polyphenol TA not only improved the dispersibility of Fe_3O_4 nanoparticles, but also enhanced the adsorption performance via the formation of hydrogen bonds. And the abundant surface hydroxyl groups could facilitate the inner-sphere complexation between iron and adsorbed species. The removal mechanism between UiO-66 shell and the adsorbates was mainly manipulated by the formed Zr—O—As and Zr—O—Sb bonds. Based on the adsorption performance, it was concluded that Fe_3O_4@TA@UiO-66 is a promising adsorbent to treat contaminated water containing As and Sb. More importantly, the magnetic microsphere could be easily separated from the aqueous media after water treatment within two minutes. This study is also

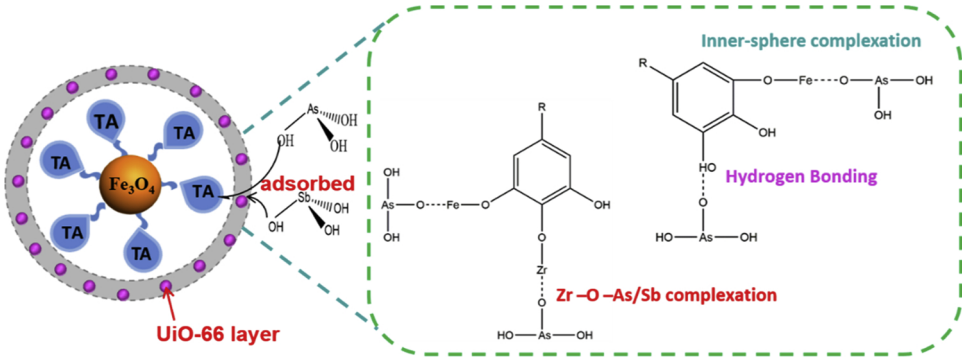

Fig. 6. Core-shell structure of Fe_3O_4@TA@UiO-66 and adsorption mechanism towards As(III) and Sb(III).

inspired to design other magnetic nanocomposite about UiO-66 analogues for the removal of contaminants from water.

Acknowledgements

This research was supported by Natural Science Foundation of Shandong Province (ZR2019QD019), Key Technology Research and Development Project of Shandong Province (2016GGX102005), and Program for Taishan Scholar of Shandong Province.

Appendix A. Supplementary data

Supplementary material related to this article can be found, in the online version, at doi:https://doi.org/10.1016/j.jhazmat.2019.05.114.

References

[1] M. Filella, N. Belzile, Y.W. Chen, Antimony in the environment a review focused on natural waters I. Occurrence, Earth—Sci. Rev. 57 (2002) 125–176.
[2] J. Luo, C. Hu, X. Meng, J. Crittenden, J. Qu, P. Peng, Antimony removal from aqueous solution using novel α-MnO_2 nanofibers: equilibrium, kinetic, and density functional theory studies, ACS Sustain. Chem. Eng. 5 (2017) 2255–2264.
[3] R.G. Cooper, A.P. Harrison, The exposure to and health effects of antimony, J. Occup. Environ. Med. 13 (2009) 3–10.
[4] S. Sundar, J. Chakravarty, Antimony toxicity, Int. J. Environ. Res. Pub. Health 7 (2010) 4267–4277.
[5] S. Yamamura, J. Bartram, M. Csanady, H.G. Gorchev, A. Redekopp, Drinking Water Guidelines and Standards, World Health Organization, Geneva, Switzerland, 2003.
[6] S.C. Wilson, P.V. Lockwood, P.M. Ashley, M. Tighe, The chemistry and behaviour of antimony in the soil environment with comparisons to arsenic: a critical review, Environ. Pollut. 158 (2010) 1169–1181.
[7] D.I. Fox, T. Pichler, D.H. Yeh, N.A. Alcantar, Removing heavy metals in water: the interaction of cactus mucilage and arsenate (As(V)), Environ. Sci. Technol. 46 (2012) 4553–4559.
[8] H. Lu, Z. Zhu, H. Zhang, J. Zhu, Y. Qiu, Simultaneous removal of arsenate and antimonate in simulated and practical water samples by adsorption onto Zn/Fe layered double hydroxide, Chem. Eng. J. 276 (2015) 365–375.
[9] S.-H. Lee, M. Tanaka, Y. Takahashi, K.-W. Kim, Enhanced adsorption of arsenate and antimonate by calcined Mg/Al layered double hydroxide: investigation of comparative adsorption mechanism by surface characterization, Chemosphere 211 (2018) 903–911.
[10] V.T. Luong, E.E.C. Kurz, U. Hellriegel, T.L. Luu, J. Hoinkis, J. Bundschuh, Iron-based subsurface arsenic removal technologies by aeration: a review of the current state and future prospects, Water Res. 133 (2018) 110–122.
[11] Y. Xie, C. Chen, X. Ren, X. Wang, H. Wang, X. Wang, Emerging natural and tailored materials for uranium-contaminated water treatment and environmental remediation, Prog. Mater. Sci. (2019) 180–234.
[12] B. Dousova, M. Lhotka, J. Filip, D. Kolousek, Removal of arsenate and antimonate by acid-treated Fe-rich clays, J. Hazard. Mater. 357 (2018) 440–448.
[13] B. Lan, Y. Wang, X. Wang, X. Zhou, Y. Kang, L. Li, Aqueous arsenic (As) and antimony (Sb) removal by potassium ferrate, Chem. Eng. J. 292 (2016) 389–397.
[14] P.A. Nishad, A. Bhaskarapillai, S. Velmurugan, Enhancing the antimony sorption properties of nano titania-chitosan beads using epichlorohydrin as the crosslinker, J. Hazard. Mater. 334 (2017) 160–167.
[15] P.A. Nishad, A. Bhaskarapillai, S. Velmurugan, Nano-titania-crosslinked chitosan composite as a superior sorbent for antimony (III) and (V), Carbohydr. Polym. 108 (2014) 169–175.
[16] P.A. Nishad, A. Bhaskarapillai, S. Velmurugan, Removal of antimony over nano titania–impregnated epichlorohydrin-crosslinked chitosan beads from a typical decontamination formulation, Nucl. Technol. 197 (2017) 88–98.
[17] B. Liu, M. Jian, H. Wang, G. Zhang, R. Liu, X. Zhang, J. Qu, Comparing adsorption of arsenic and antimony from single-solute and bi-solute aqueous systems onto ZIF-8, Colloid Surf. A 538 (2018) 164–172.
[18] P.A. Kobielska, A.J. Howarth, O.K. Farha, S. Nayak, Metal–organic frameworks for heavy metal removal from water, Coord. Chem. Rev. 358 (2018) 92–107.
[19] S. Dhaka, R. Kumar, A. Deep, M.B. Kurade, S.-W. Ji, B.-H. Jeon, Metal–organic frameworks (MOFs) for the removal of emerging contaminants from aquatic environments, Coord. Chem. Rev. 380 (2019) 330–352.
[20] J. Li, X. Wang, G. Zhao, C. Chen, Z. Chai, A. Alsaedi, T. Hayat, X. Wang, Metal–organic framework-based materials: superior adsorbents for the capture of toxic and radioactive metal ions, Chem. Soc. Rev. 47 (2018) 2322–2356.
[21] Y. Wu, H. Pang, Y. Liu, X. Wang, S. Yu, D. Fu, J. Chen, X. Wang, Environmental remediation of heavy metal ions by novel-nanomaterials: a review, Environ. Pollut. 246 (2019) 608–620.
[22] N.A. Khan, Z. Hasan, S.H. Jhung, Adsorptive removal of hazardous materials using metal-organic frameworks (MOFs): a review, J. Hazard. Mater. 244 (2013) 444–456.
[23] C.O. Audu, H.G.T. Nguyen, C.-Y. Chang, M.J. Katz, L. Mao, O.K. Farha, J.T. Hupp, S.T. Nguyen, The dual capture of As^{V} and As^{III} by UiO-66 and analogues, Chem. Sci. 7 (2016) 6492–6498.
[24] M. Feng, P. Zhang, H.-C. Zhou, V.K. Sharma, Water-stable metal-organic frameworks for aqueous removal of heavy metals and radionuclides: a review, Chemosphere (2018) 783–800.
[25] D. Bůžek, J. Demel, K. Lang, Zirconium metal–organic framework UiO-66: stability in an aqueous environment and its relevance for organophosphate degradation, Inorg. Chem. 57 (2018) 14290–14297.
[26] C. Tian, J. Zhao, X. Ou, J. Wan, Y. Cai, Z. Lin, Z. Dang, B. Xing, Enhanced adsorption of p-Arsanilic acid from water by amine-modified UiO-67 as examined using extended X-ray absorption fine structure, X-ray photoelectron spectroscopy, and density functional theory calculations, Environ. Sci. Technol. 52 (2018) 3466–3475.
[27] J. Wei, W. Zhang, W. Pan, C. Li, W. Sun, Experimental and theoretical investigations on Se(IV) and Se(VI) adsorption to UiO-66-based metal–organic frameworks, Environ. Sci.—Nano (2018) 1441–1453.
[28] Y. He, Y.P. Tang, D. Ma, T.-S. Chung, UiO-66 incorporated thin-film nanocomposite membranes for efficient selenium and arsenic removal, J. Membr. Sci. 541 (2017) 262–270.
[29] H. Hao, G. Liu, Y. Wang, B. Shi, K. Han, Y. Zhuang, Y. Kong, Simultaneous cationic Cu(II)–anionic Sb(III) removal by NH_2-Fe_3O_4-NTA core-shell magnetic nanoparticle sorbents synthesized via a facile one-pot approach, J. Hazard. Mater. 362 (2019) 246–257.
[30] X. Min, W. Yang, Y.F. Hui, C.Y. Gao, S. Dang, Z.M. Sun, Fe_3O_4@ZIF-8: a magnetic nanocomposite for highly efficient UO_2^{2+} adsorption and selective UO_2^{2+}/Ln^{3+} separation, Chem. Commun. 53 (2017) 4199–4203.
[31] L. Xu, Y. He, X. Feng, F. Dai, N. Yang, Y. Zhao, L. Chen, A comprehensive description of the threshold flux during oil/water emulsion filtration to identify sustainable flux regimes for tannic acid (TA) dip-coated poly(vinylidene fluoride) (PVDF) membranes, J. Membr. Sci. 563 (2018) 43–53.
[32] K. Atacan, M. Özacar, Characterization and immobilization of trypsin on tannic acid modified Fe3O4 nanoparticles, Colloid Surf. B 128 (2015) 227–236.
[33] R. Guo, X. Cai, H. Liu, Z. Yang, Y. Meng, F. Chen, Y. Li, B. Wang, In situ growth of metal-organic frameworks in three-dimensional aligned lumen arrays of wood for rapid and highly efficient organic pollutants removal, Environ. Sci. Technol. (2019).
[34] J. Wu, K. Chen, X. Tan, M. Feng, X. Hu, Z. Tang, X. Wang, Core-shell CMNP@PDAP nanocomposites for simultaneous removal of chromium and arsenic, Chem. Eng. J. 349 (2018) 481–490.
[35] P. Hu, Z. Zhao, X. Sun, Y. Muhammad, J. Li, S. Chen, C. Pang, T. Liao, Z. Zhao, Construction of crystal defect sites in N-coordinated UiO-66 via mechanochemical in-situ N-doping strategy for highly selective adsorption of cationic dyes, Chem. Eng. J. 356 (2019) 329–340.
[36] C.-H. Liu, Y.-H. Chuang, T.-Y. Chen, Y. Tian, H. Li, M.-K. Wang, W. Zhang, Mechanism of arsenic adsorption on magnetite nanoparticles from water: thermodynamic and spectroscopic studies, Environ. Sci. Technol. 49 (2015) 7726–7734.
[37] C. Tian, J. Zhao, J. Zhang, S. Chu, Z. Dang, Z. Lin, B. Xing, Enhanced removal of roxarsone by Fe_3O_4@3D graphene nanocomposites: synergistic adsorption and mechanism, Environ. Sci.—Nano 4 (2017) 2134–2143.
[38] J. Li, X. Li, T. Hayat, A. Alsaedi, C. Chen, Screening of zirconium-based metal–organic frameworks for efficient simultaneous removal of antimonite (Sb(III)) and antimonate (Sb(V)) from aqueous solution, ACS Sustain. Chem. Eng. 5 (2017) 11496–11503.
[39] K. Yang, J. Zhou, Z. Lou, X. Zhou, Y. Liu, Y. Li, S.A. Baig, X. Xu, Removal of Sb(V) from aqueous solutions using Fe-Mn binary oxides: the influence of iron oxides forms and the role of manganese oxides, Chem. Eng. J. 354 (2018) 577–588.
[40] He Xingyu, Min Xiaobo, L. Xubiao, Efficient removal of antimony(III, V) from contaminated water by amino modification of zirconium metal-organic framework with mechanism study, J. Chem. Eng. Data 62 (2017) 1519–1529.
[41] Z. Lv, Q. Fan, Y. Xie, Z. Chen, A. Alsaedi, T. Hayat, X. Wang, C. Chen, MOFs-derived magnetic chestnut shell-like hollow sphere NiO/Ni@C composites and their removal performance for arsenic(V), Chem. Eng. J. 362 (2019) 413–421.
[42] L. Valenzano, B. Civalleri, S. Chavan, S. Bordiga, M.H. Nilsen, S. Jakobsen, K.P. Lillerud, C. Lamberti, Disclosing the complex structure of UiO-66 metal organic framework: a synergic combination of experiment and theory, Chem. Mater. 23 (2011) 1700–1718.
[43] S. Mitsunobu, T. Harada, Y. Takahashi, Comparison of antimony behavior with that of arsenic under various soil redox conditions, Environ. Sci. Technol. 40 (2006) 7270–7276.
[44] P. Qi, T. Pichler, Sequential and simultaneous adsorption of Sb(III) and Sb(V) on ferrihydrite: implications for oxidation and competition, Chemosphere 145 (2016) 55–60.
[45] C.D. Wagner, W.M. Riggs, L.E. Davis, J.F. Moulder, G.E. Muilenberg, Handbook of X-Ray Photoelectron Spectroscopy, (1979).